PRODUCTION OF OXYGEN FROM LUNAR ILMENITE

Y. ZHAO and F. SHADMAN
University of Arizona

The kinetics and mechanism of reduction of ilmenite by carbon monoxide as well as hydrogen at 800 to 1100°C were investigated. The temporal profiles of conversion have a sigmoidal shape and indicate the presence of three different stages (induction, acceleration and deceleration) during CO reduction at all temperatures and H2 reduction at the temperatures below 876°C. The apparent activation energies based on the initial rates are 29.6 kcal/mole for CO reduction and 22.3 kcal/mole for H_2 reduction, respectively. The reaction is first order with respect to carbon monoxide and hydrogen under the experimental conditions studied. Both SEM and EDX analyses show that the diffusion of Fe product away from the reaction front and through the TiO_2 phase, followed by the nucleation and growth of a separate Fe phase are important steps in both reduction processes. The main difference between these two reactions is that TiO_2 can be reduced to lower oxides of titanium by hydrogen at temperatures higher than 876°C, and the reduction rate of ilmenite by H_2 is much faster than that of ilmenite by CO. A novel process flow sheet for carbothermal reduction process is also presented.

I. INTRODUCTION

The most useful material to produce on the Moon is oxygen for propellant (Cole and Segal 1964). There is a significant amount of oxygen on the Moon although very little is readily available as water or gaseous oxygen. The only practical source of oxygen on the lunar surface is igneous materials which contain typically 40 to 50% oxygen as oxides. The major minerals present in these rocks are ilmenite (the most abundant opaque mineral in lunar rocks), anorthite, and olivine. The igneous rocks have been pre-crushed by meteoritic bombardments to form regolith, the lunar equivalent of soil. This reduces the need for crushing and simplifies the mining and separation problem greatly.

Extraction of oxygen from iron oxide, as in the lunar ilmenite is of particular interest because it is energetically more favorable than extraction from silicon, aluminum, titanium, calcium or magnesium oxides. Iron oxide reduction is also attractive because of its potential for producing iron as a co-product. In addition, Agosto (1985) has concluded that ilmenite can be obtained from lunar soil at high purity using electrostatic separation techniques. A number of processes have been suggested for oxygen production from ilmenite in lunar regolith. Most of these processes require imported reagents to be recycled in the process. Therefore, low loss per pass is a critical factor and requirement for process feasibility. Among the proposed

processes, the hydrogen and carbothermal reduction of ilmenite appear very promising. Hydrogen reduction has a relatively simple process configuration; the individual steps are relatively well studied. However, the major problem is large heating and cooling loads required to condense the water and then heat the H_2 back up to its reaction temperature. Handling and storage of large amounts of hydrogen is also a problem.

Most of the available literature describes investigations on naturally occurring ores using carbon, CO or H_2 as reducing agents (Wouterlood 1979; Poggi et al. 1973; Bardi et al. 1987). From a fundamental point of view, the results of such studies are difficult to interpret because of the complex nature of the ores and the presence of many components. While CO might be an intermediate compound in any carbothermal reduction (Gupta et al. 1987; El-Guindy and Davenport 1970), the fundamental kinetics and mechanism of ilmenite reduction with CO are not clearly known. Poggi and Charette (1973) studied the reduction of synthetic ilmenite by carbon monoxide. However, their results are difficult to interpret because under the conditions used in their studies, carbon was also formed from CO disproportionation and participated in the ilmenite reduction. El-Guindy and Davenport (1970) investigated the reduction of synthetic ilmenite with graphite and discovered that the reduction starts at ~860°C at the contact points between the reactants. Up to 1020°C solid state reduction appears to be the main reaction mechanism, while above this temperature a rate increase has been observed and has been attributed to a change of mechanism to gaseous reduction of ilmenite by regenerated CO.

Briggs and Sacco (1988) studied the reduction of ilmenite by hydrogen at 600°C and 800°C. The ilmenite used in their study contained ~8% ferric iron. They found that some preoxidation of ilmenite by oxygen prior to reduction can decrease the complete reduction time of samples. During preoxidation, the ilmenite is converted to pseudobrookite (Fe_2TiO_5) and rutile. The single crystals of ilmenite are converted, therefore, into a polycrystalline array of pseudobrookite and a fine dispersion of rutile (Barnes and Pickles 1988). Carbotek (1988) has developed a fluidized-bed reactor for the reduction of ilmenite by hydrogen at the temperature between 900°C and 1000°C. Terrestrial ilmenite was used in this study. They demonstrated the feasibility of producing oxygen from terrestrial ilmenite by first reducing the terrestrial ilmenite and then electrolyzing water to produce oxygen and hydrogen which is returned to the reactor. They also reported that the reaction is first order with respect to hydrogen under their experimental conditions. Bardi et al. (1987) investigated the kinetics of hydrogen reduction of Norwegian ilmenite ore powders. The electron microprobe analysis of the reduced Norwegian ilmenite grains showed the existence of a segregated iron phase present as spheroidal nodules and a TiO_2 phase present as vein-like arrangements. Their optical microscopic study on sections of synthetically prepared $FeTiO_3$ showed separate reacted and unreacted zones in the sample particles.

Donnelly (1970) reduced ilmenite beach sands using a mixture of hydrogen and carbon monoxide and found that diluting the hydrogen reducing gas

with CO decreases the rate of reduction of the iron oxide. The lowering of the rate of reduction is attributed to the water gas shift reaction. In view of the presence of both CO and H_2 in ilmenite reduction process based on the use of carbonaceous waste as a carbon source, the kinetics and the mechanism of synthetic ilmenite reduction by H_2/CO is currently under study in our laboratory.

In this chapter, the principal aim is to describe the reduction of ilmenite by carbon monoxide and hydrogen under conditions where the original ilmenite and the final products are well characterized. The emphasis is on ilmenite with no ferric impurities present. This is important in applying the results to the reduction of lunar ilmenite. Section II describes the experimental setup. The kinetics and mechanism of ilmenite reduction by carbon monoxide and hydrogen are considered in Secs. III and IV, respectively. Section V deals with the comparison of CO and H_2 reduction of ilmenite and a new process flowsheet for a novel carbothermal reduction process of ilmenite. Finally, various conclusions are given in Sec. VI.

II. EXPERIMENTAL APPROACH

A schematic of the experimental apparatus is shown in Fig. 1. The main components of this system are an electronic microbalance (Cahn Instruments, Inc., Model 1000), a quartz flow through reactor with inlet and outlet, and a movable furnace with a PID controller. The composition of gaseous reactants and products was determined using an infrared analyzer and a gas chromatograph. Ilmenite was used in the form of thin flakes pressed from powder. Samples were suspended from the microbalance, which monitored weight changes during the course of an experiment. A thermocouple was used to monitor the temperature of the reactor around the flake. All experiments were performed under isothermal conditions. For the CO reduction, the reducing gas entering the reactor contained CO, CO_2 and N_2. The ratio of CO to CO_2 was always maintained at 99 to prevent carbon deposition due to the CO disproportionation reaction (Jones 1975; Shomate 1946). The gas flow was varied from 105 to 260 std.cc/min. For H_2 reduction, the reducing gas contained H_2 and N_2. The gas flow ranged from 260 to 660 std.cc/min.

Samples of starting material were prepared by cold pressing approximately 0.270 g of $FeTiO_3$ powder (with particles size $<45\ \mu m$) in a die at 14,500 psi for 5 minutes to form disks. The disks were then cut into flakes approximately 10 mm by 8 mm. The thickness of the disks was 0.60 mm except for experiments conducted to determine the effect of intergranular diffusion resistance (transport through void space among grain particles).

Each experiment was started by first purging the reactor system at room temperature to reduce the concentration of oxygen to levels below 25 ppm. The reducing gas was then introduced into the reactor. To initiate the reduction, the furnace was raised rapidly. Within three minutes the temperature in

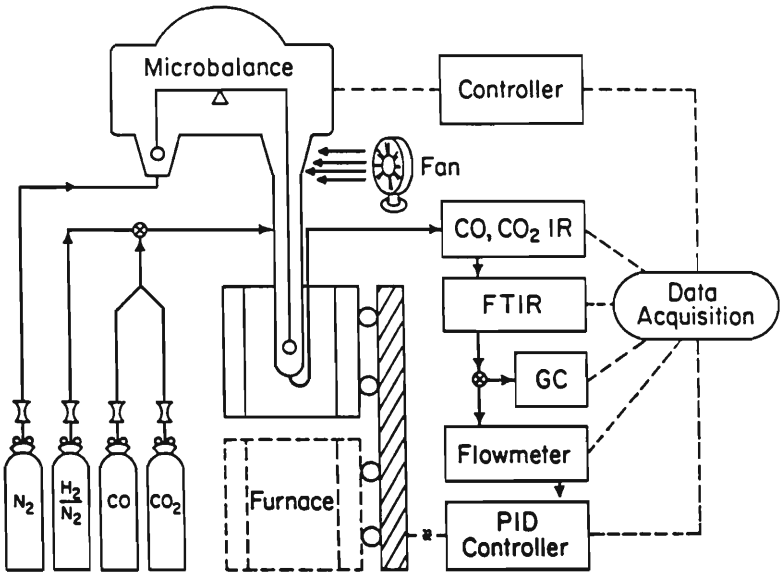

Figure 1. Schematic diagram of the reactor system. GC=gas chromatograph, IR=non-dispersive infrared analyzer, FTIR=Fourier transform infrared spectrometer.

the reactor was within 1% of the set point temperature. The experiments were terminated at a desired conversion by rapidly lowering the furnace.

Several techniques were used for chemical analysis and characterization of the starting and reduced samples. Mossbauer spectroscopy was employed to determine the oxidation state of iron in our synthetic ilmenite. X-ray diffraction (XRD) was used to identify the different crystalline phases in the starting material and products. High-resolution scanning electron microscopy (SEM) and energy-dispersive X-ray (EDX) analyses were employed to examine the polished cross section of both partially and completely reduced samples and to determine the elements present in each phase. For SEM and EDX analyses, the samples were mounted in an epoxy resin and polished to expose the cross section of the grains.

III. REDUCTION OF ILEMITE WITH CARBON MONOXIDE

The experimental results of CO reduction of ilmenite are presented in this section. The impurity content of our synthetic ilmenite used in this study is given in Table I. The XRD pattern of our synthetic ilmenite, as shown in Fig. 2a, suggests that the sample contains only the $FeTiO_3$ crystalline phase. A typical two-line Mossbauer spectrum of the sample, shown in Fig. 3b, confirms that the iron in the synthetic ilmenite is in the form of Fe^{++}. This

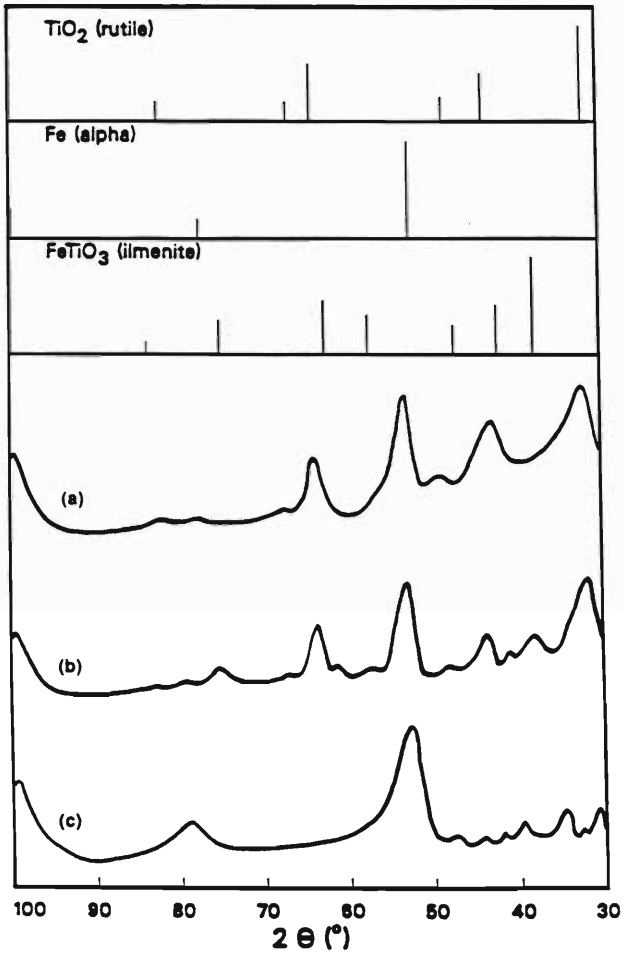

Figure 2. (a) X-ray diffraction spectrum of synthetic ilmenite. (b) X-ray diffraction spectrum of synthetic ilmenite after complete reduction. T = 900, 1000, 1100°C. (c) X-ray diffraction spectrum of synthetic ilmenite after partial reduction. T = 1000°C.

represents the oxidation state of iron in lunar ilmenite. The six-line Mossbauer spectrum of hematite or Fe_2O_3 is given in Fig. 3a.

For each experiment, the total sample weight loss was obtained based on the continuous microbalance measurement and the total amount of CO_2 was given by the on-line infrared gas analyzer, which is capable of continuously monitoring the concentration of CO_2 in the gas phase. It is found that these two measurements agree well with following stoichiometry:

$$FeTiO_3(s) + CO(g) = CO_2(g) + Fe(s) + TiO_2(s). \quad (1)$$

The first set of experiments were conducted to determine the effect of interphase transport resistance around the flakes. The experiments were conducted at the highest temperature (1100°C) with 13% CO. As shown in Fig. 4, the interphase resistance is not important if the flow rate is at least 260

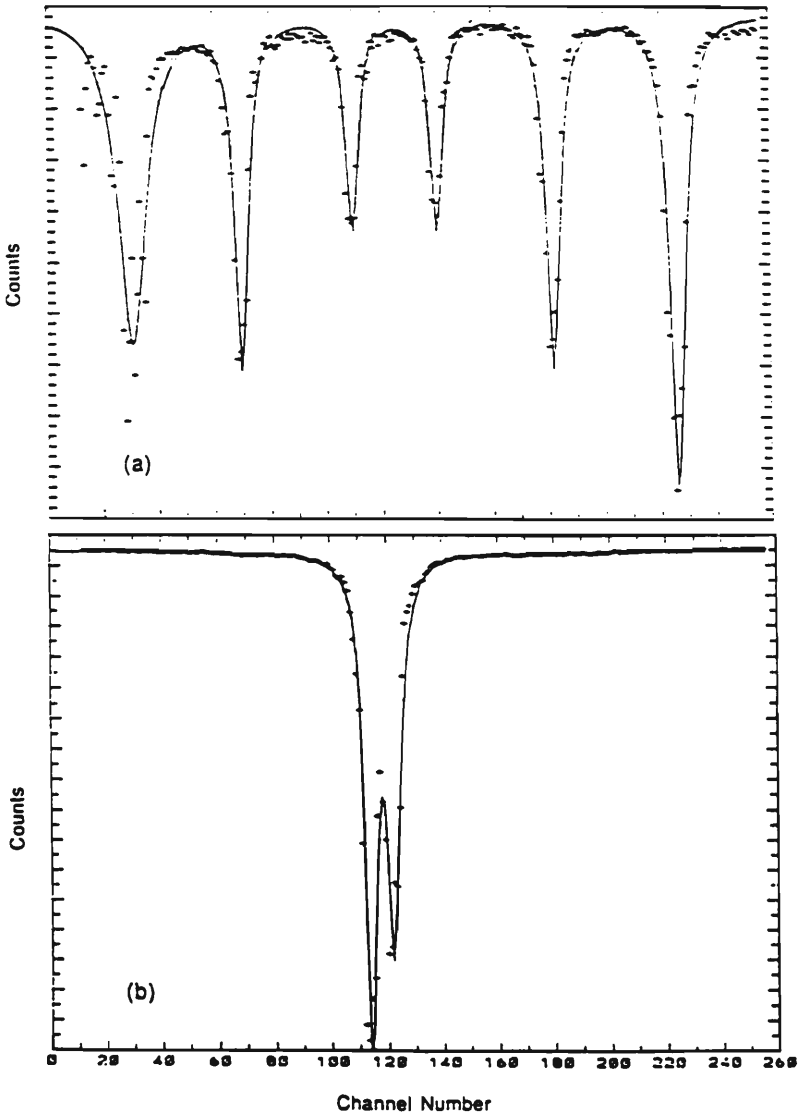

Figure 3. (a) Mossbauer velocity spectrum for hematite. (b) Mossbauer velocity spectrum for synthetic ilmenite.

std.cc/min. At temperatures below 1100°C, the interphase resistance will be even less significant.

The second set of experiments were to determine the effects of intergranular diffusion of CO on the kinetics. These experiments were conducted at the highest temperature (1100°C) with 23% CO and at a gas flow rate of 260 std.cc/min. As shown in Fig. 5, the intergranular diffusion of CO does not affect the reduction kinetics if the flake thickness is less than 0.60 mm.

To find the reaction order, a series of experiments were conducted at 13% and 23% CO concentration at 900, 1000 and 1100°C. The results, shown in Fig. 6, show that the reaction order with respect to carbon monoxide is unity

TABLE I
Maximum Impurity Content in the
As-Received Synthetic Ilmenite

Impurity	Maximum Concentration (Wt. %)
Al	0.001
Ca	0.01
Cr	0.001
Cu	0.01
Mg	0.001
Si	0.1

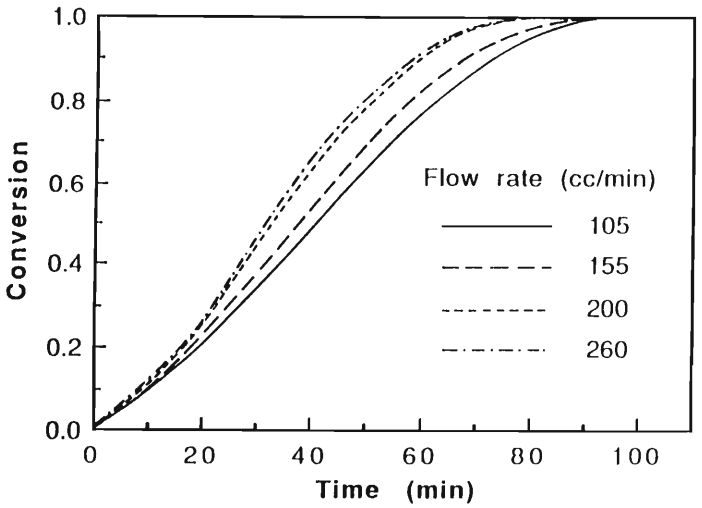

Figure 4. The effect of gas flow rate on the reduction rate of ilmenite. [CO]=13%, $T = 1100°$.

in this range of temperature and CO concentration. Therefore, the rate of reaction can be written as

$$r = k(T, X)C_{CO} \tag{2}$$

where rate is expressed in [mg reacted/original mg/min] and C_{CO} is in gmole/liter.

The effect of temperature on the reaction rate at various conversions is shown in Fig. 7. The apparent activation energy was 18, 14 and 10 kcal/gmole at 10%, 30% and 50% conversion level, respectively. As conversion increases, the thickness of the TiO_2 product layer in grain particles increases. This increases the diffusional resistance against the CO transport into the grain particles. The higher diffusional resistance causes a decrease in the apparent activation energy.

Isothermal weight loss measurements were performed at 900, 1000 and 1100°C. The temporal profiles of conversion at these three temperatures and

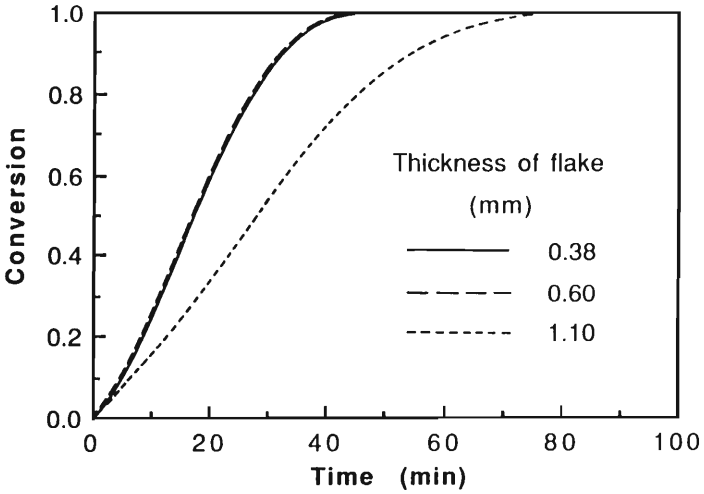

Figure 5. The effect of flake thickness on the reduction rate of ilmenite. [CO]=23%, $T = 1100°C$.

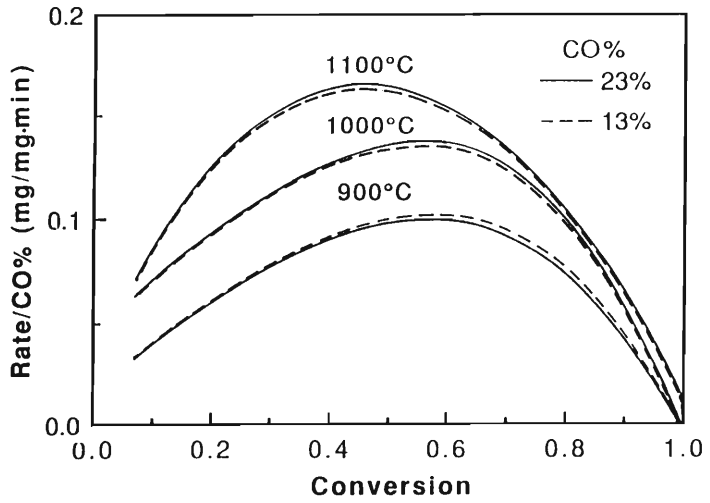

Figure 6. The effect of CO concentration on the reduction rate of ilmenite.

CO concentration of 23% are shown in Fig. 8. These profiles have a sigmoidal shape and indicate the presence of three different stages (induction, acceleration and deceleration) during the reduction reaction.

To gain insight into the mechanism of the ilmenite reduction, particularly in relation to the observed three stages, samples of both completely and partially reduced ilmenite were analyzed using various analytical techniques. In particular, a combination of optical microscopy, SEM, EDX and XRD analyses provided very useful information on the nature and distribution of various phases including the products Fe and TiO_2.

A SEM secondary electron micrograph of the polished cross section of an ilmenite flake after partial reduction at 1000°C is shown in Fig. 9a. The

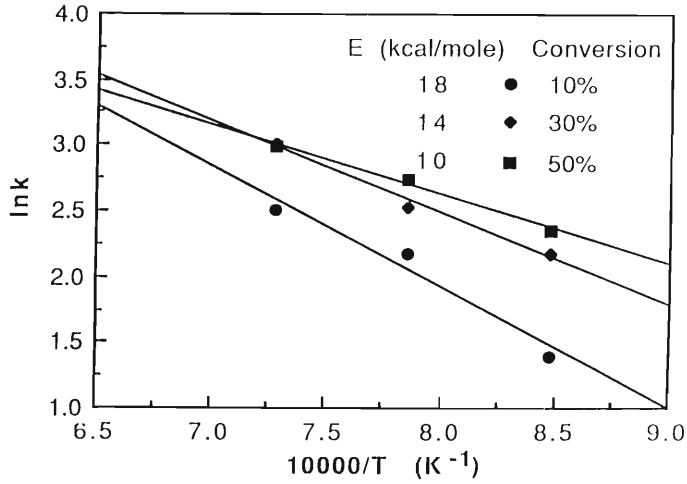

Figure 7. Values of apparent activation energy at 10, 30, and 50% conversion.

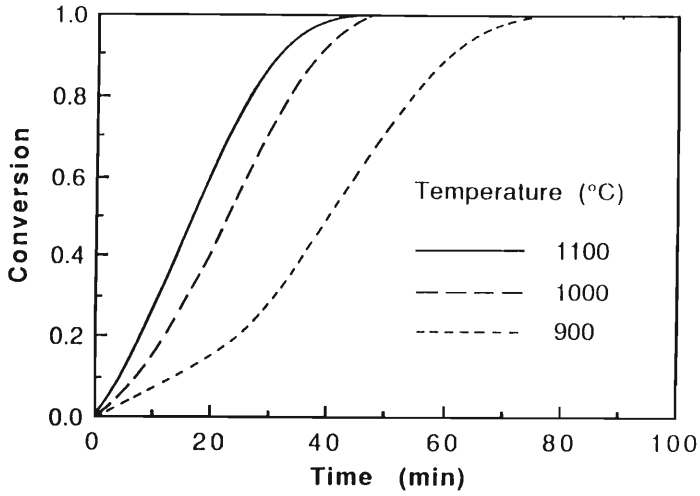

Figure 8. The effect of temperature on the reduction rate of ilmenite. CO%=23.

micrograph reveals three distinct regions which appear as bright, light gray and dark gray phases. In order to identify the phases present, quantitative EDX was performed at spots marked in Fig. 9a. The observations show that the bright phase is primarily iron, the dark gray phase is made up of titanium dioxide and the light gray phase is unreacted $FeTiO_3$. These results suggest that there is a strong tendency towards the segregation of the products iron and titanium dioxide and that iron diffuses to the grain boundaries through the TiO_2 layer during the reduction. This finding has important implications for product separation for recovery of Fe and TiO_2. Because the reduction temperatures are much lower than the melting point of TiO_2, it is expected that the TiO_2 product exists in polycrystal form. As shown in Fig. 9a, it appears that the reaction in the grain particles proceeds according to the shrinking

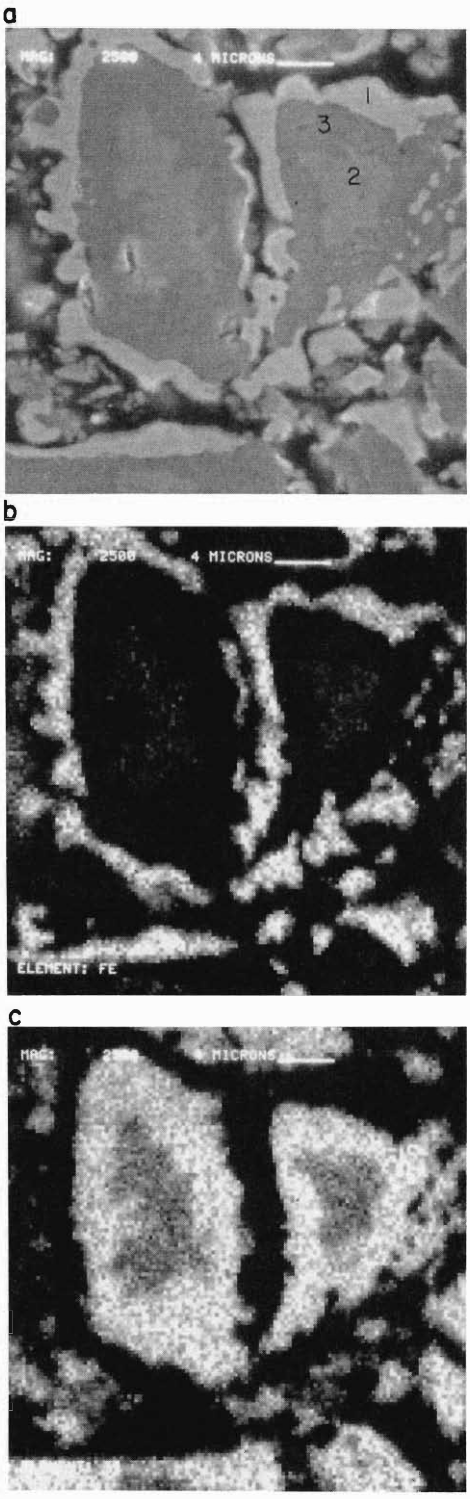

Figure 9. (a) SEM secondary electron micrograph of the polished cross section of ilmenite flake after partial reduction. $T = 1000°C$; magnification=2500X; point 1: 3.1 atom% Ti, 96.9 atom% Fe; point 2: 51.6 atom% Ti, 48.4 atom% Fe; point 3: 98.9 atom% Ti, 1.1 atom% Fe. (b) Fe Kα X-ray map of the cross section shown in 9a. (c) Ti Kα X-ray map of the cross section shown in 9a.

unreacted core model. This result is expected because the grain particles of synthetic ilmenite are nearly nonporous, whereas the product TiO_2 is porous. The corresponding X-ray Kα map of iron and titanium, as shown in Figs. 9b and 9c, confirm the shrinking core configuration.

The polished cross-sections of synthetic ilmenite flakes after complete reduction at 900 and 1100°C were also examined by SEM and EDX. The results obtained, as shown in Figs. 10 and 11, indicate that a similar mechanism of reduction is involved. However, the coalescence of grains is observed in the flakes reduced at 1100°C, which is apparently due to the sintering of iron. The results of EDX analyses on these samples indicate that, the phase enriched in titanium is depleted in iron and vice versa. This confirms the high degree of segregation of product Fe and TiO_2.

The XRD spectra of both partially and completely reduced samples are shown in Fig. 2b and 2c. The phases present after complete reduction at 900, 1000, and 1100°C were iron and titanium dioxide and those present after partial reduction at 1000°C were iron, titanium dioxide and unreacted ilmenite. These findings confirm the data obtained from EDX analysis.

The various observations described here all point to a mechanism consisting of the following main steps for the reaction in each grain:

1. Diffusion of CO through the porous product layer of TiO_2 towards the unreacted core of grain particles;
2. Reaction of CO with the ilmenite core to produce TiO_2 and Fe;
3. Migration of Fe through the TiO_2 layer away from the unreacted core towards the grain boundary;
4. Formation of iron nuclei and their subsequent growth outside and around the reacted grain particles.

Steps 3 and 4 result in almost complete segregation of the two solid products iron and titanium dioxide in the scale of grains.

Using this proposed mechanism, the three stages observed during conversion can be described as follows:

a. Induction stage: this represents the initial stage of the reduction process and corresponds to the formation of iron nuclei. At this stage, most of iron reduced from $FeTiO_3$ is in the matrix of TiO_2. The duration of this period is temperature sensitive, decreasing from 15 minutes at 900°C to five minutes at 1100°C.
b. Acceleration stage: in this stage, the iron nuclei formed during the induction stage as well as those that may form subsequently grow. As more Fe diffuses out and pores in TiO_2 layer open up; this allows more CO to diffuse into the matrix of TiO_2 and react with $FeTiO_3$. The rate of reduction increases and reaches a maximum. Iron cannot be a catalyst leading to rapid rate during this stage of the reaction. If iron does catalyze the reaction, then the induction stage would not exist and the maximum rate would be observed at a very low conversion.

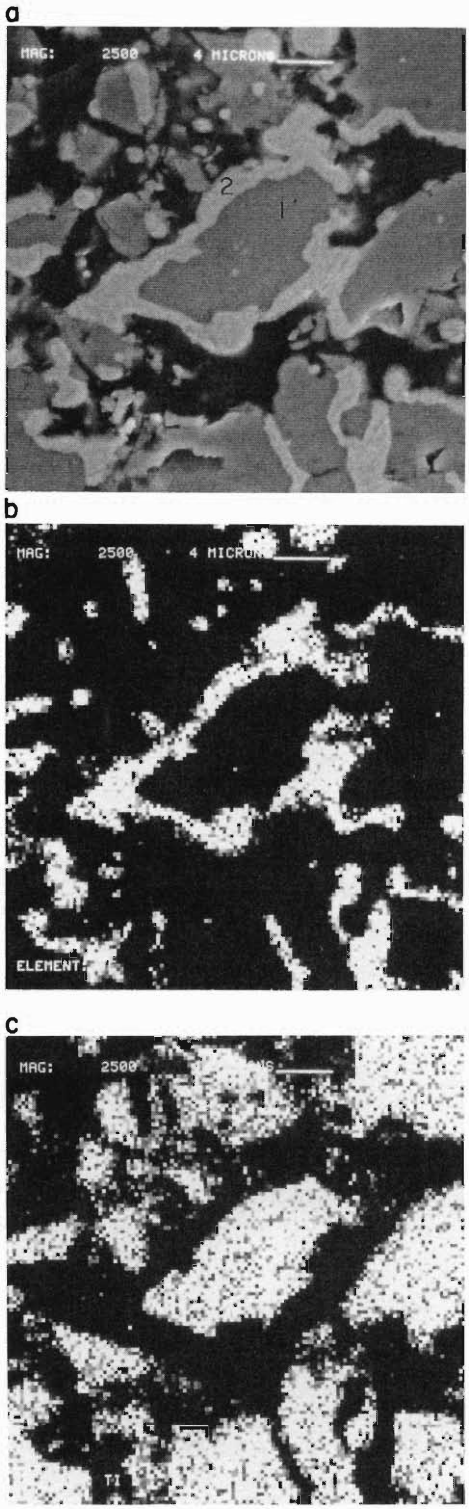

Figure 10. (a) SEM secondary electron micrograph of the polished cross section of ilmenite flake after complete reduction. $T = 900°C$, magnification=2500X. Point 1: 99.0 atom% Ti, 1.0 atom% Fe; point 2: 5.4 atom% Ti, 94.6 atom% Fe (b) Fe Kα X-ray map of the cross section shown in 10a (c) Ti Kα X-ray map of the cross section shown in 10a.

c. Deceleration stage: depletion of $FeTiO_3$ results in a decrease in the rate of reduction.

For a direct observation of the effect of iron nucleation on the rate, in a series of experiments, a known amount of iron powder with particle size $<45\ \mu m$ was added to ilmenite powder before pressing. As shown in Fig. 12, the addition of iron significantly reduced the length of induction period. This confirms the suggestion that the low rate during the initial induction period is due to the absence of sufficient iron nuclei. This causes slow transport of iron away from the reaction front and inhibition of CO contact with the unreacted $FeTiO_3$.

It appears that only Poggi et al. (1973) has examined the CO reduction of ilmenite. The synthetic ilmenite sample in their study is in the form of fused briquette with the porosity of 1%, whereas the sample in our study has porosity of 30%. In addition, the CO disproportionation was not considered in their work. These make it difficult to compare the results. They found the activation energy to be 14.1 kcal per mole in the temperature range 900 to 1100°C.

IV. REDUCTION OF ILMENITE WITH HYDROGEN

A. Experimental Results

Initially, some experiments were conducted to determine the effect of transport resistance in the interphase around the flakes. The experiments were conducted at the highest temperature (1014°C) with 3.4% H_2. The results showed that the interphase resistance is not important if the flow rate is at least 660 std.cc/min. At temperatures below 1014°C, the interphase resistance is even less significant.

The results in Fig. 13 show the effect of H_2 concentration on the reaction at 945°C. The H_2 concentration was varied between 3.4% and 14.7% in N_2 atmosphere. As expected, an increase in the hydrogen concentration results in an increase in the rate and a decrease in the time required to attain certain fractional weight loss, which is defined as the ratio of weight loss of the sample to initial weight of the sample. The reaction order with respect to H_2 is established using the runs which were not influenced by diffusion in the ilmenite flake. The results, shown in Fig. 14, indicate that the reaction order is unity in the H_2 concentration range of 3.4% to 14.7% at 807°C and 876°C. This confirms the first order kinetics assumption presented in the theoretical section.

Isothermal weight loss measurements were performed at 807, 876, 945 and 1014°C. The temporal profiles of conversion at these four temperatures and H_2 concentration of 3.4% are shown in Fig. 15. The profile at 807°C has a sigmoidal shape and indicates the presence of three different stages (induction, acceleration and deceleration) during the reduction reaction. The profiles at 876°C, 945°C and 1014°C do not have these three stages. As

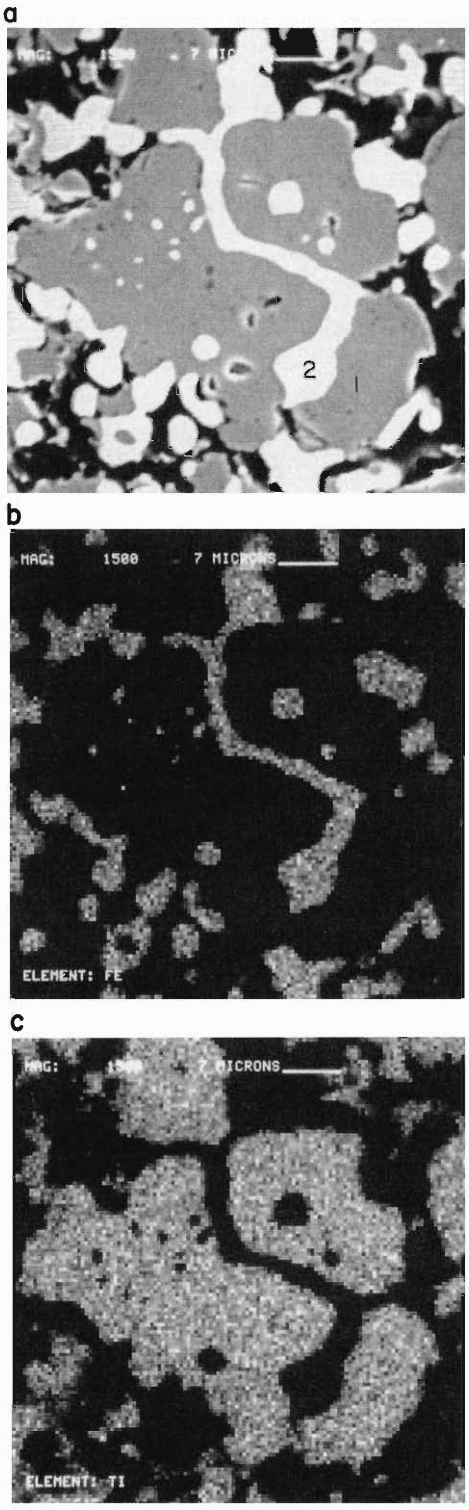

Figure 11. (a) SEM secondary electron micrograph of the polished cross section of ilmenite flake after complete reduction. $T = 1100°C$, magnification=2500X. Point 1: 99.0 atom% Ti, 1.0 atom% Fe; point 2: 2.5 atom% Ti, 97.5% Fe (b) Fe Kα X-ray map of the cross section shown in 11a. (c) Ti Kα X-ray map of the cross section shown in 11a.

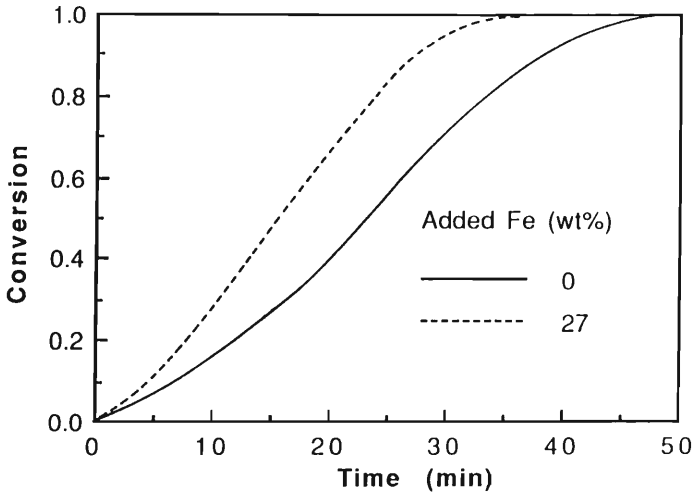

Figure 12. The effect of iron addition on the reduction rate of ilmenite. CO%=23, $T = 1000°C$.

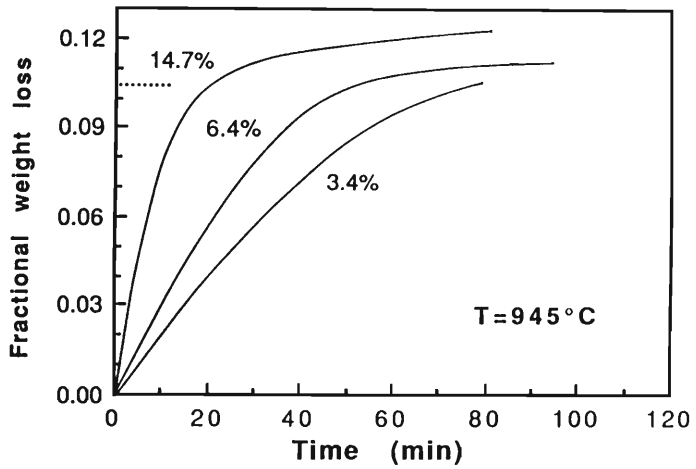

Figure 13. Effect of hydrogen concentration on the reduction of ilmenite; —— complete iron metallization.

shown in Fig. 15, the time required to attain the weight loss corresponding to complete iron metallization when all the iron in ilmenite is reduced to metallic iron, is 210 minutes at 807°C and 52 minutes 1014°C with 3.4% H_2. The effect of temperature on the reaction rate is shown in Fig. 16. The apparent activation energy calculated based on initial rates is 22.3 kcal/mole.

SEM backscattered electron micrographs of the polished cross section of ilmenite flake after partial reduction at 1014°C and 807°C are shown in Figs. 17a and 18a. The micrographs reveal three distinct regions which appear as bright, light gray and dark gray phases. In order to identify these phases, quantitative EDX was performed at spots marked in Figs. 17a and 18a. These results and the XRD observations (to be discussed later) show that the bright

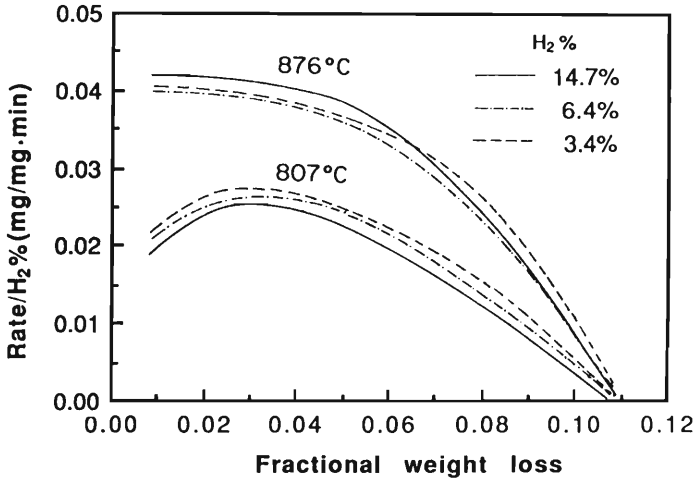

Figure 14. Effect of hydrogen concentration on the reduction rate of ilmenite.

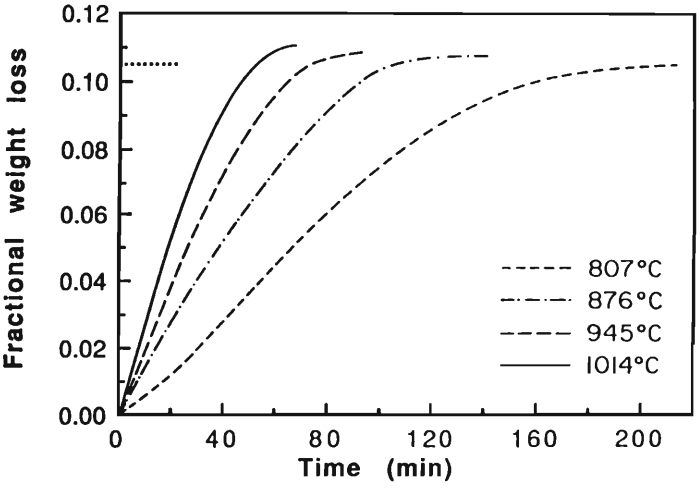

Figure 15. Effect of temperature on the reduction rate of ilmenite: H_2=2.4%; —, complete iron metallization.

phase is primarily iron; the dark gray phase is titanium dioxide and the light gray phase is unreacted $FeTiO_3$.

Figure 17a and 18b indicate that the reaction in the grain particles proceeds according to the shrinking core model. The corresponding X-ray map of iron and titanium, shown in Figs. 17b, 17c, 18b and 18c, confirm the shrinking core configuration, which is very similar to CO reduction.

The results in Sec. III showed that the reduction of TiO_2 by CO did not take place at any appreciable rate in the temperature range between 800°C to 1100°C. However, the experimental results for the ilmenite reduction by hydrogen in Fig. 13 show that the total weight loss of the sample exceeds the weight loss corresponding to the complete iron metallization. This indicates

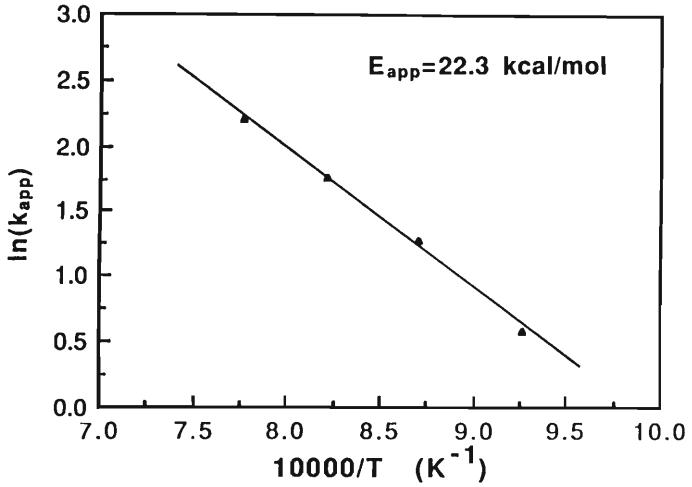

Figure 16. Temperature dependence of the apparent rate coefficient.

that titanium dioxide can be reduced by hydrogen in the temperature range of 876°C and 1014°C. The rate of reduction of titanium dioxide depends on both the hydrogen concentration and the reaction time. The reduction of titanium dioxide has practical significance in the production of oxygen from lunar ilmenite, because 67% of oxygen in ilmenite is bound to titanium.

In order to understand the mechanism of titania reduction by hydrogen, the electron microprobe with wavelength dispersive X-ray analysis was employed to determine the atomic ratio of oxygen to titanium in the reduced titanium dioxide phase. The analyzed area of the grain in the sample reduced at 1014°C is shown in Fig. 19. For each sample, the analyses for titanium and oxygen were performed across the two polished grains. One is located at the edge of the flake; the other is located at the center. The results obtained from these two grains are very similar. The results showing the extent of reduction of TiO_2 are given by Fig. 20 and indicate that the reduction of titania took place throughout the titanium dioxide matrix in each grain. These observations suggest that the reduction of titanium dioxide in each grain and across the flake is kinetically controlled.

Another important point related to the reduction of TiO_2 is its inception relative to iron reduction. To further study this, two partially reduced samples were prepared at 1014°C and 14.7% H_2, the first one at 35% conversion and the second one at 70% conversion. The results of WDX analysis showed that the TiO_2 phases in both samples had not been reduced at either conversions. These results indicate that the reduction of TiO_2 does not occur to any significant extent as long as iron metallization is not completed. It is speculated that this is related to inhibition effect of water vapor as the reaction product. The equilibrium constants of TiO_2 reduction by hydrogen in the temperature range of interest are much smaller than those of ilmenite reduction. During ilmenite reduction (iron metallization), the concentration of water vapor inside the

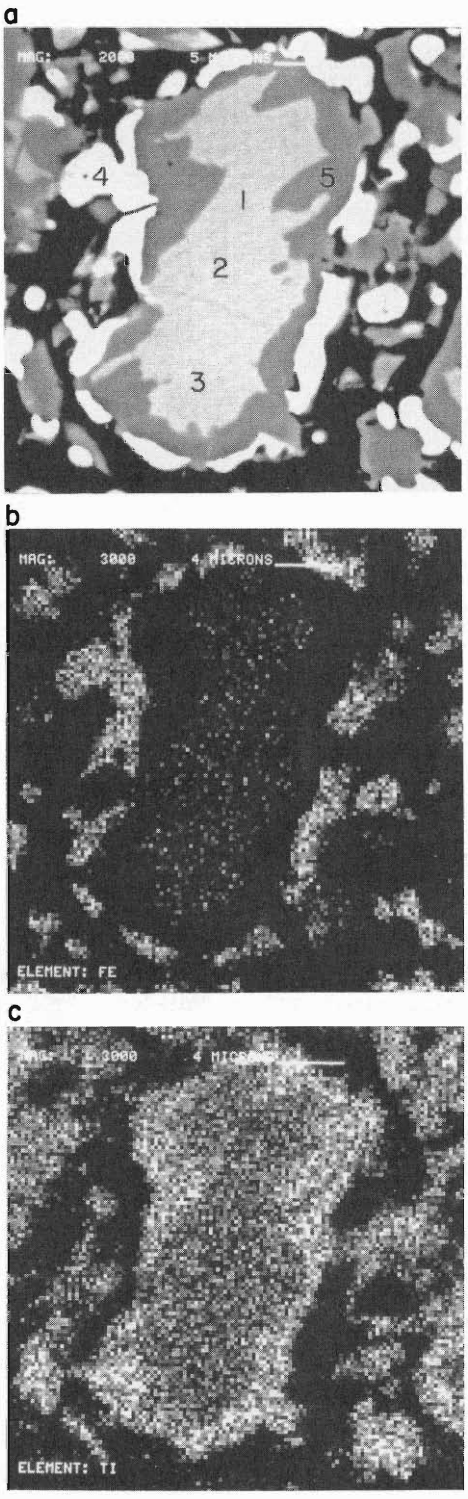

Figure 17. (a) Backscattered electron micrograph of the polished cross section of ilmenite flake after partial reduction. $T = 1014°C$, magnification=2000X. Point concentrations in atom% are as follows: Point 1: Ti 50; Fe 50. Point 2: Ti 51; Fe 49. Point 3: Ti 51; Fe 49. Point 4: Ti 2; Fe 98. Point 5: Ti 96; Fe 4. (b) Fe Kα X-ray map of the cross section shown in 17a. (c) Ti Kα X-ray map of the cross section shown in 17a.

TiO_2 pores is high enough to inhibit the TiO_2 reduction. However, as iron metallization approaches completion, the inhibition effect decreases and TiO_2 reduction starts.

The XRD spectra of partially reduced samples are shown in Fig. 21b. The phases present after partial reduction at 807°C and 1014°C are iron, titanium dioxide and unreacted ilmenite. Figure 21a is the XRD spectrum of sample reduced at 807°C with "complete iron metallization," and indicates the presence of Fe and TiO_2. The samples reduced at 876°C, 945°C and 1014°C with 13% fractional weight loss were also analyzed using XRD. The patterns, shown in Fig. 21c, indicate that all the peaks of TiO_2 phases disappeared, which confirms the reduction of TiO_2 by H_2.

The sigmoidal profiles of conversion and the three stages observed during ilmenite reduction are similar to what is observed in the CO reduction in the Sec. III. However, the induction stage in the H_2 reduction of ilmenite is less significant than that in CO reduction. This is because hydrogen diffusivity in the pores is significantly larger than CO diffusivity. Therefore, the effect of pore blockage on H_2 reduction is less than that on the CO reduction.

B. Theoretical Modelling

A mathematical model is formulated to describe the simultaneous reaction and diffusion that occur in the ilmenite flakes used in the experimental part of this study. The flakes were uniform and thin; therefore, the geometry assumed for mathematical modeling is that of an infinitely long and wide slab. This configuration was selected because it gives the desired information on the kinetics of ilmenite reduction without complications of sample shape. Thin flakes are also suitable for polishing as needed in the microprobe studies. It is assumed that the flakes consist of spherical and equal-sized grain particles of ilmenite. Based on the SEM micrographs and image analysis of grains in a flake, the overall size of a flake and the size of an individual grain do not change significantly during the reaction.

The reactions considered are as follows:

$$FeTiO_3(s) + H_2(g) = H_2O(g) + TiO_2(s) \tag{3}$$

or

$$FeTiO_3(s) + CO(g) = CO_2(g) + Fe(s) + TiO_2(s) \tag{4}$$

The following additional assumptions are made:

1. The pseudosteady state approximation is appropriate for describing the concentration of the gaseous species within a flake;
2. The system is isothermal;
3. The effective diffusivities of gaseous reactant and product are equal and uniform throughout the flake;
4. The reaction is first order with respect to H_2, H_2O, CO, and CO_2;
5. The grain particles have little porosity and react following a shrinking-core mechanism.

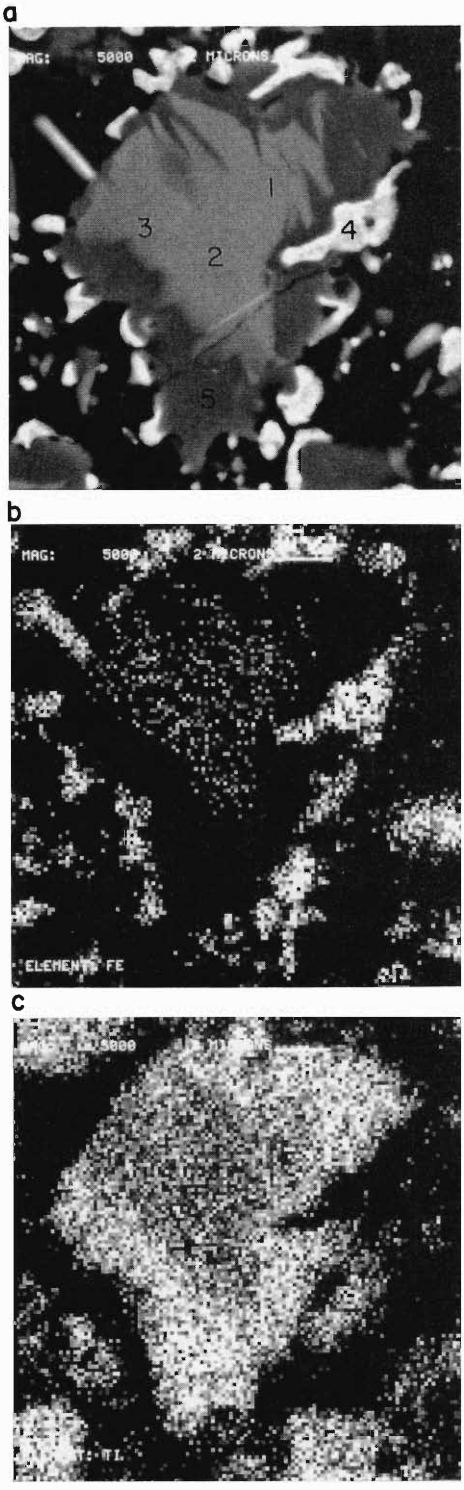

Figure 18. (a) Backscattered electron micrograph of the polished cross section of ilmenite flake after partial reduction. $T = 807°C$, magnification=5000X. Point concentrations in atom% are as follows Point 1: Ti 50; Fe 50. Point 2: Ti 50; Fe 50. Point 3: Ti 51; Fe 49. Point 4: Ti 5; Fe 95. Point 5: Ti 99; Fe 1. (b) Fe Kα X-ray map of the cross section shown in 18a. (c) Ti Kα X-ray map of the cross section shown in 18a.

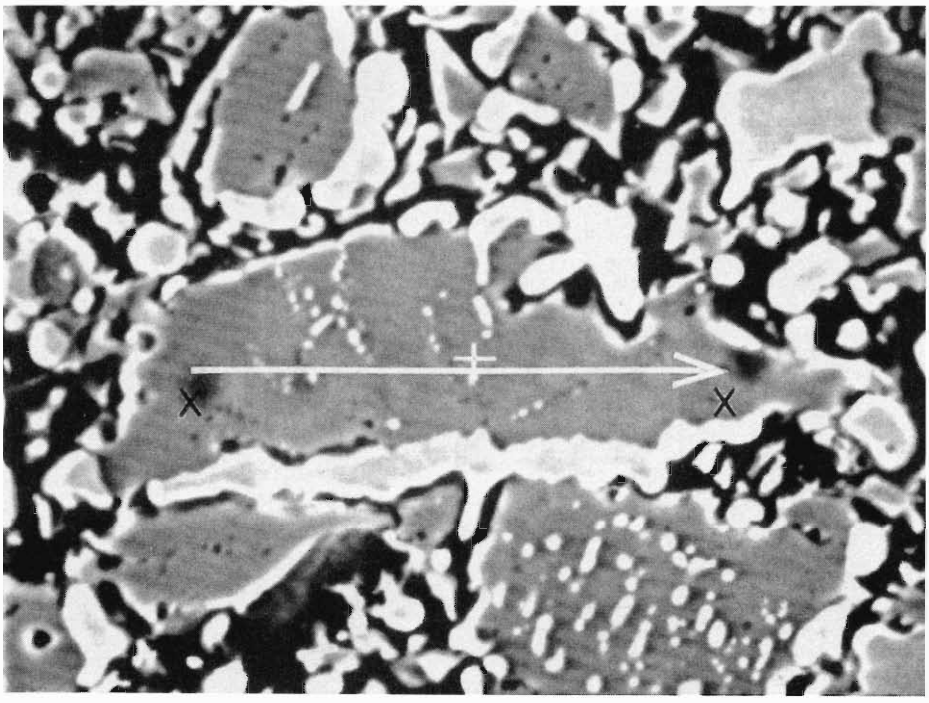

Figure 19. Backscattered electron micrograph of a reduced TiO_2 phase.

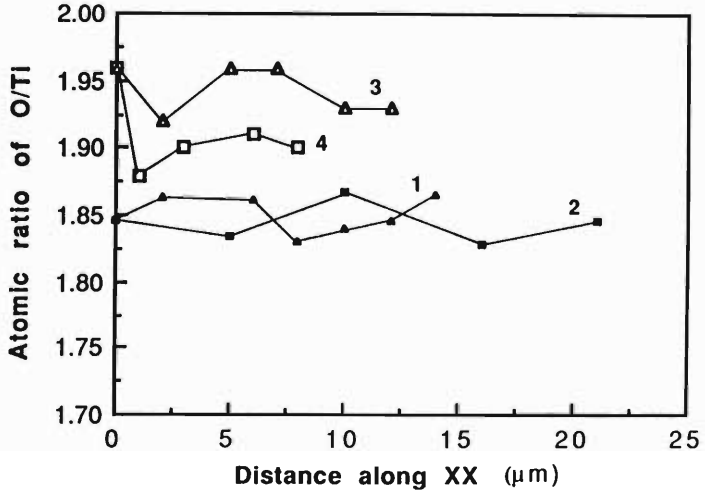

Figure 20. Variation in the oxygen to titanium atomic ratio in flakes. 1: sample 1, edge (Fig. 11), $T = 1014°C$; 2: sample 1, center $T = 1014°C$; 3: sample 2, edge, $T = 876°C$; 4: sample 2, center, $T = 876°C$.

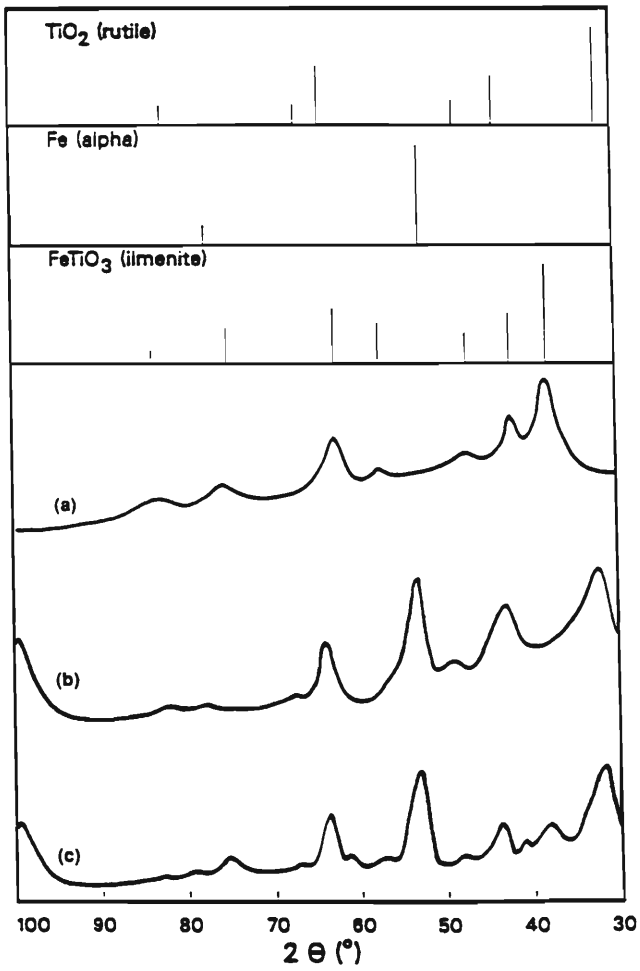

Figure 21. X-ray diffraction spectrum of: (a) ilmenite, complete iron metallization at 807°C; (b) ilmenite, partially reduced at 807°C or 1014°C; (c) ilmenite, complete iron metallization and partial reduction of TiO_2 at 876°C, 945°C and 1014°C.

The conservation equations for hydrogen or CO, A and water or CO_2, C, can be written as follows:

$$D_e \nabla^2 C_A - R_A = 0 \tag{5}$$

$$D_e \nabla^2 C_c + R_A = 0. \tag{6}$$

The local rate of reaction based on the grain particles is given by the standard shrinking core model:

$$-\rho_s \frac{dr_c}{dt} = k \frac{C_A - C_c/K}{1 + \frac{k(1+1/K)}{D_{eg}} \left(1 - \frac{r_c}{r_s}\right) r_c}. \tag{7}$$

Dividing Eq. (6) by K and subtracting from Eq. (5) gives:

$$D_e \nabla^2 (C_A - C_c/K) - R_A(1 + 1/K) = 0. \tag{8}$$

The initial and the boundary conditions for (7) and (8) are: at $t = 0, r_c = r_s$; at $Z = L, C_A - C_c/K = C_{Ab} - C_{cb}/K$; at $Z = 0, \frac{d(C_A - C_c/K)}{dz} = 0$.

An expression can be obtained for the local rate of reaction R_A. For a flake in this study, R_A is given by:

$$R_A = 3\frac{\frac{r_c^2}{r_s^3}(1-\epsilon)k(C_A - C_c/K)}{1 + \frac{k(1+1/K)}{D_{eg}} r_c \left(1 - \frac{r_c}{r_s}\right)}. \tag{9}$$

The local conversion can be related to the unreacted grain radius as follows:

$$X_B = 1 - \left(\frac{r_c}{r_s}\right)^3. \tag{10}$$

The overall conversion for a flake is given by:

$$X = \left(\frac{1}{L}\right)\int_0^L X_B \mathrm{d}Z. \tag{11}$$

It has been shown by Sohn (1974) that the solution to the model can be described by the following relationship:

Time required to attain a certain conversion $\approx$	Time required to attain the same conversion in the absence of resistance due to intrapellet diffusion	+Time required to attain the same conversion under the control of intrapellet diffusion

$$t^* \approx f(X) + \sigma_g^2 \cdot g(X) + \sigma^2 \cdot p(X) \tag{12}$$

$$t^* = \frac{k}{\rho_s r_s}(C_{AB} - C_{Cb}/K)t \tag{13}$$

$$\sigma_g^2 = \frac{k r_s}{6 D_{eg}}(1 + 1/K) \tag{14}$$

$$\sigma^2 = L^2 \frac{(1-\epsilon)k}{2 D_e r_s}(1 + 1/K) \tag{15}$$

$$f(X) = 1 - (1 - X)^{1/3} \tag{16}$$

$$g(X) = 1 - 3(1 - X)^{2/3} + 2(1 - X) \tag{17}$$

$$p(x) = X^2. \tag{18}$$

The terms on the right side of Eq. (12) are the asymptotic expressions which can be related to conversion as shown in Eqs. (16)–(18). The results

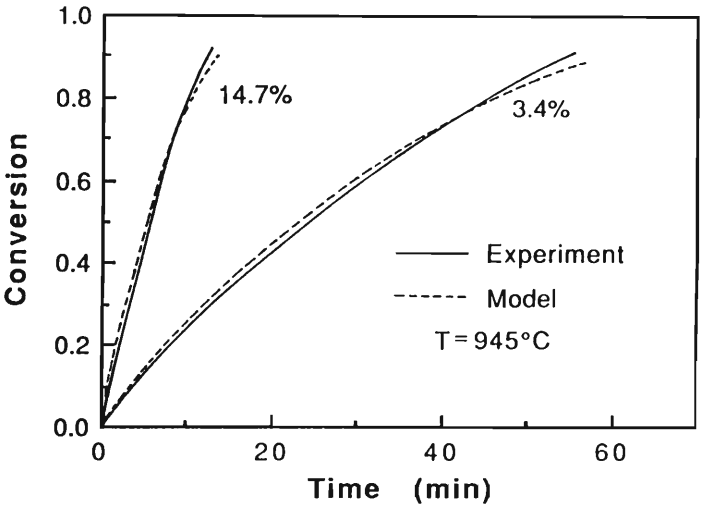

Figure 22. Comparison of experimental data with model predictions: H_2=3.4% and 14.7%.

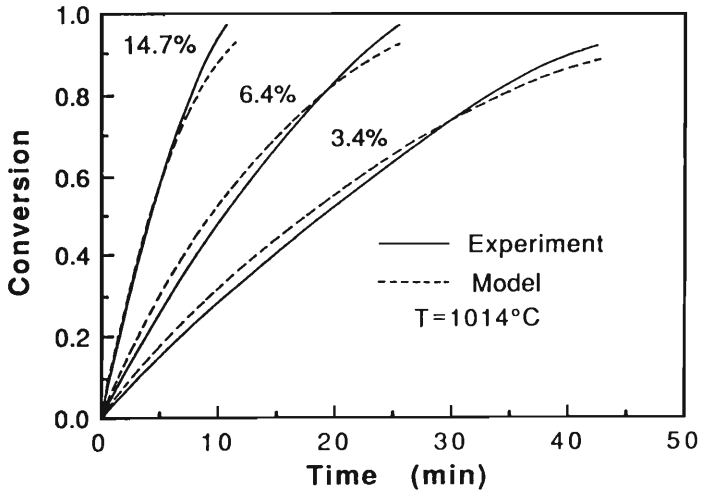

Figure 23. Comparison of experimental data with model predictions: H_2=3.4%, 6.4% and 14.7%.

obtained by this method are very close to the exact solution that must be obtained numerically Sohn (1974). The closed-form solution of this problem is discussed in more detail by Sohn (1978).

The model formulated has been used to extract intrinsic reaction rate constant of H_2 reduction of ilmenite from the experimental measurements. A list of parameters used in the model is given in Table II. The model agrees well with the experimental measurements. Sample results for model predictions at 945°C and 1014°C are shown in Figs. 22 and 23. The Arrhenius plot based on the intrinsic reaction rate constants is shown in Fig. 24. The intrinsic activation energy for the reaction on ilmenite core is 16.9 kcal/mole, which is lower than the apparent activation energy discussed earlier. The reason is

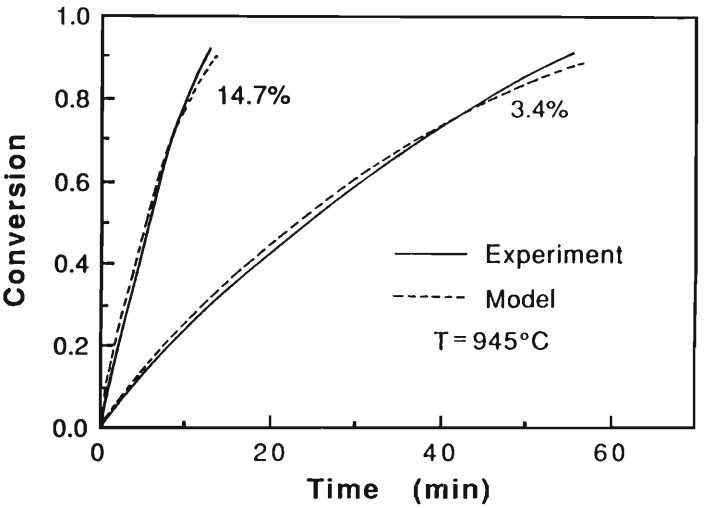

Figure 22. Comparison of experimental data with model predictions: H_2=3.4% and 14.7%.

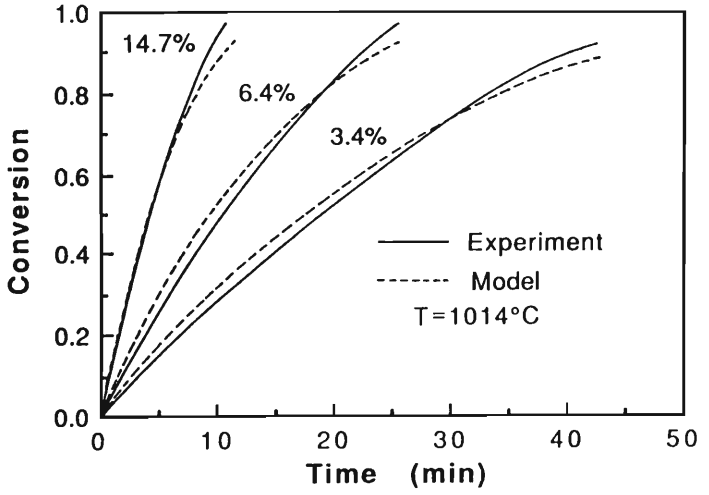

Figure 23. Comparison of experimental data with model predictions: H_2=3.4%, 6.4% and 14.7%.

obtained by this method are very close to the exact solution that must be obtained numerically Sohn (1974). The closed-form solution of this problem is discussed in more detail by Sohn (1978).

The model formulated has been used to extract intrinsic reaction rate constant of H_2 reduction of ilmenite from the experimental measurements. A list of parameters used in the model is given in Table II. The model agrees well with the experimental measurements. Sample results for model predictions at 945°C and 1014°C are shown in Figs. 22 and 23. The Arrhenius plot based on the intrinsic reaction rate constants is shown in Fig. 24. The intrinsic activation energy for the reaction on ilmenite core is 16.9 kcal/mole, which is lower than the apparent activation energy discussed earlier. The reason is

of carbonaceous waste as a carbon source. Therefore, it is very important to compare the reduction of ilmenite by CO with the reduction of ilmenite by H_2.

The mechanisms of ilmenite reduction by H_2 and CO are very similar. Both reactions involve the migration and nucleation of iron, leading to the complete segregation of iron from TiO_2. The main difference between these two reactions is that TiO_2 can be reduced to lower oxides of titanium by hydrogen and the reduction rate of ilmenite by H_2 is much faster than that of ilmenite by CO.

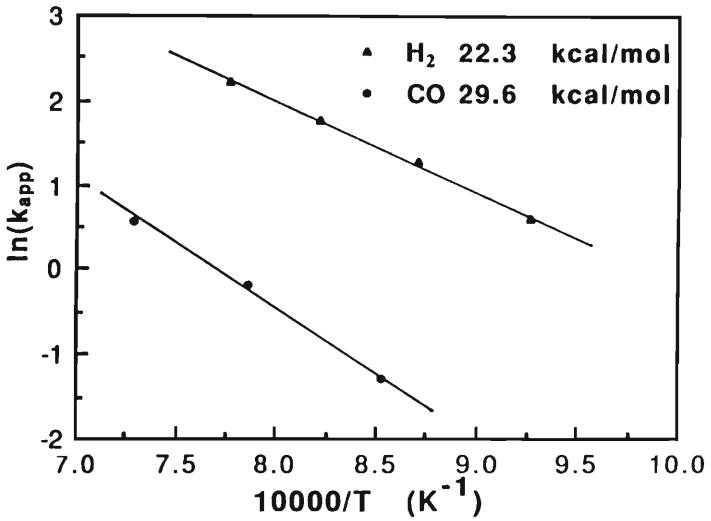

Figure 25. Temperature dependence of the apparent rate coefficient.

The effect of temperature on both reactions is shown in Fig. 25. The apparent activation energy for H_2 reduction of ilmenite is 22.3 kcal/mol, whereas the apparent activation energy for CO reduction of ilmenite is 29.6 kcal/mol. This suggests that the reduction of ilmenite by CO is more sensitive to temperature than that by H_2.

In order to determine the effect of reducing agents on the reaction rate and the time corresponding to the "complete iron metallization," two sets of experiments were conducted at the same condition. The results in Figs. 26 and 27 show that the initial reaction rates of ilmenite reduction by H_2 are 8.6 and 11.3 times larger than those by CO reduction at 1000°C and 900°C, respectively. The times corresponding to the "complete iron metallization" are 12.5 minutes and 34 minutes at 1000°C and 900°C for H_2 reduction of ilmenite, whereas, for the CO reduction of ilmenite, times are 95 minutes and 135 minutes at 1000°C and 900°C.

The flowsheet for a novel carbothermal reduction process has been recently developed and is shown in Fig. 28. The components and their functions in this flowsheet are described as follows:

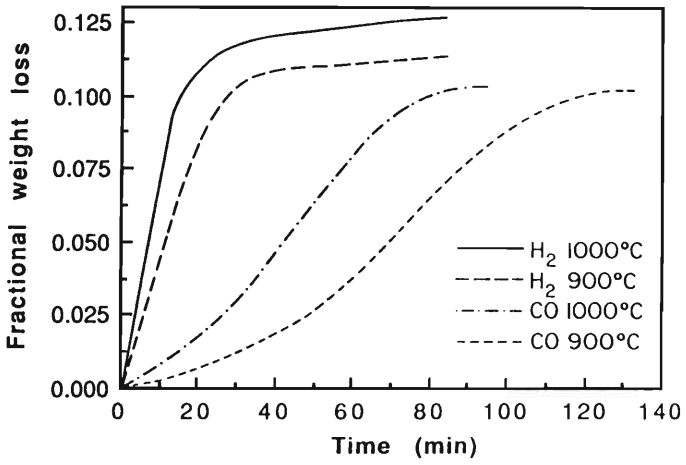

Figure 26. Effect of reducing agents on the reduction of ilmenite: [H_2] or [CO] (10^3 mol/L)—T(°C); 1.15—1000; 1.24—900.

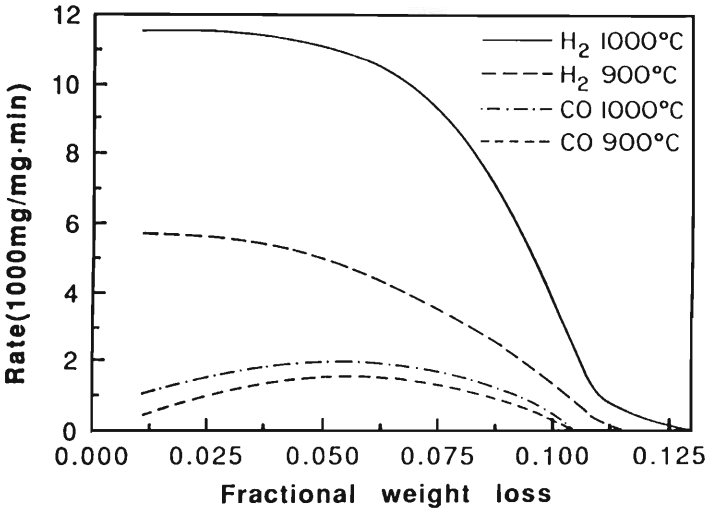

Figure 27. Effect of reducing agents on the reduction rate of ilmenite: [H_2] or [CO] (10^3 mol/L)—T(°C); 1.15—1000; 1.24—900.

1. Carbon monoxide generation section.
2. Reactor with lower operating temperature: this reactor is designed to deposit carbon on lunar ilmenite. The thermodynamic calculation indicates that the deposit of carbon on lunar ilmenite can increase the oxygen yield significantly.
3. Reactor with higher operating temperature: this reactor is to carry out the carbothermal reduction of lunar ilmenite. The major products in this reactor are Fe, TiO_2, CO and CO_2.
4. Oxygen recovery from CO_2 by electrolysis.

The staged reactor system with carbon deposition and reduction occurring

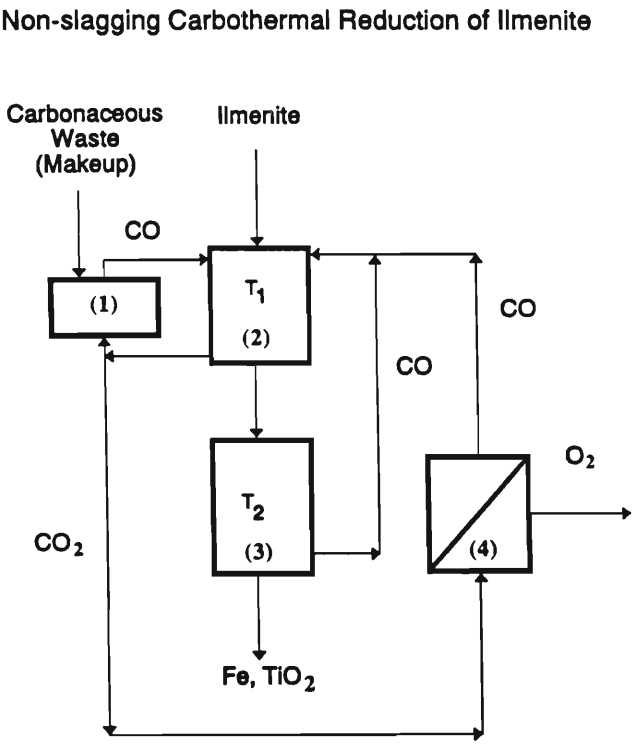

Figure 28. Flowsheet for a novel carbothermal reduction process.

at two different temperatures is a novel scheme that overcomes the inherent yield deficiency in other ilmenite reduction process (Shadman et al. 1991; Zhao and Shadman 1990).

VI. CONCLUSIONS

The reduction of ilmenite grains by H_2 and CO follow a shrinking core configuration and consists of four primary steps: diffusion of H_2 or CO through the product layer TiO_2 reaction of H_2 or CO with the ilmenite, diffusion of iron out of the TiO_2 pores, and nucleation and growth of metallic iron outside the ilmenite grain particles.

The temporal profiles of conversion of ilmenite reduction with H_2 at temperatures below 876°C and by CO at all temperatures exhibit three stages during the reaction: induction, acceleration and deceleration. The induction period is due to the slow transport of iron out of the pores resulting from insufficient iron nuclei at the onset the reduction process.

The apparent activation energy based on initial rate for the ilmenite reduction with H_2 is 22.3 kcal/mole, whereas the apparent activation energy of CO reduction of ilmenite is 29.6 kcal/mole.

The comparison of two reduction processes indicate that the reduction rate of ilmenite by hydrogen is much faster and less sensitive to temperature

than CO reduction. Moreover, TiO_2 can be reduced to lower oxides of titanium by H_2 at temperature higher than 876°C.

The proposed theoretical model agrees well with the experimental measurements and can be used for design and parametric study.

NOMENCLATURE

C_A: concentration of H_2, gmol/cc
C_{Ab}: concentration of H_2 in bulk gas, gmol/cc
C_C: concentration of H_2O, gmol/cc C_{Cb}: concentration of H2O in bulk gas, gmol/cc
D_e: effective diffusivity in macro-pores in flake, cm^2/sec
D_{eg}: effective diffusivity in the micro-pores of product layer in each grain, cm^2/sec
E: intrinsic activation energy, kcal/mole
$f(X)$: function defined by Eq. (15)
k: surface reaction rate coefficient, cm/sec
K: equilibrium constant
L: half thickness of the slab, cm
$g(X)$: function defined by Eq. (16)
$p(X)$: function defined by Eq. (17)
R_A: reaction rate, gmol H_2/cc bulk flake, sec
r_c: radius of unreacted core in each grain, cm
r_s: radius of grain, cm
t: time, sec
t^*: dimensionless time, defined by Eq. (12)
T: temperature, °K
X_B: conversion of each grain
X: overall conversion of flake
Z: distance from the center of the slab, cm

Greek Symbols

ϵ: macro porosity
ρ_s: ilmenite molar density, gmol/cm^3
σ: generalized gas-solid reaction modulus defined by Eq. (13)
σ_g: dimensionless modulus for the reaction of the grain, defined by Eq. (13)

Acknowledgment. This research was supported by NASA/UA Center for Utilization of Local Planetary Resources at the University of Arizona. The NASA/UA Graduate College Fellowship for Y. Zhao is gratefully acknowledged. Discussions with Dr. A. H. Cutler were very helpful in this study.

REFERENCES

Agosto, W. N. 1985. Electrostatic concentration of lunar soil minerals. In *Lunar Bases and Space Activities of the 21st Century*, ed. W. W. Mendell (Houston: Lunar and Planetary Inst.), pp. 453–464.

Bardi, G., Gozzi, D., and Stranges, S. 1987. High temperature reduction kinetics of ilmenite by hydrogen. *Mater. Chem. Phys.* 17:325–341.

Barnes, C., and Pickles, C. A. 1988. A thermogravimetric studies of the catalytic effect of alkali carbonates on the reduction of ilmenite. *High Temp. Tech.* 6(4):195–201.

Briggs, R. A., and Sacco, J. A. 1988. Oxidation and reduction of ilmenite; application to oxygen production on the Moon. In *Papers Presented to the Symp. on Lunar Bases and Space Activities in the 21st Century*, April 5–7, Houston, Tex., LPI Contrib. 652, p. 34.

Cole, D. M., and Segal, R. 1964. Rocket propellants from the Moon. *Astronaut. Aeronaut.* 2:56–63.

Donnelly, R. P. 1970. Reduction of iron oxide beach sands in ilmenite. *Australian Mining*, March, 1970.

El-Guindy, M. I., and Davenport, W. G. 1970. Kinetics and mechanism of ilmenite reduction with graphite. *Metal. Trans.* 1:1729–1734.

Gupta, S. K., Rajakumar, Y., and Grieveson, P. 1987. Kinetics of reduction of ilmenite with graphite at 1000 to 1100°C. *Metal. Trans. B* 18:713–718.

Jones, D. G. 1975. Kinetics of gaseous reduction of ilmenite. *J. Appl. Chem. Biotechnol.* 25:561–582.

Poggi, D., Charette, G. G., and Rigaud, M. 1973. Reduction of ilmenite and ilmenite ores. In *Titanium Science and Technology*, eds. R. I. Jaffee and H. M. Burte (New York: Plenum), pp. 691–695.

Shadman, F., Zhao, Y., and Massieon, C. 1991. Production of oxygen from lunar ilmenite. In *Annual Progress Report: NASA/University of Arizona Center for Utilization of Local Planetary Resources* (Tucson: UA/NASA SERC), pp. IA-9–IA-68.

Shomate, C. H., Naylor, B. F., and Boericke, F. S. 1946. U. S. Bureau of Mines Report No. 3864 (Washington, D. C.: U. S. Dept. of the Interior.

Sohn, H. Y. 1974. The effect of intragrain diffusion on the reaction between a porous solid and gas. *Chem. Eng. Sci.* 29:630–634.

Sohn, H. Y. 1978. The law of additive reaction times in fluid-solid reactions. *Metal. Trans. B.* 9:89–96.

Wouterlood, H. J. 1979. The reduction of ilmenite with carbon. *J. Chem. Tech. Biotechnol.* 29:603–618.

Zhao, Y., and Shadman, F. 1990. Kinetics and mechanism of ilmenite reduction with carbon monoxide. *AIChE J.* 36(9):1443–1448.